



Contents lists available at ScienceDirect

## Urban Climate

journal homepage: <http://www.elsevier.com/locate/uclim>



# Large-eddy simulations of ventilation for thermal comfort – A parametric study of generic urban configurations with perpendicular approaching winds



Weiwen Wang<sup>a,\*</sup>, Edward Ng<sup>a,b,c</sup>, Chao Yuan<sup>d</sup>, Siegfried Raasch<sup>e</sup>

<sup>a</sup> School of Architecture, The Chinese University of Hong Kong, Hong Kong, China

<sup>b</sup> Institute of Environment, Energy and Sustainability, The Chinese University of Hong Kong, Hong Kong, China

<sup>c</sup> Institute of Future Cities, The Chinese University of Hong Kong, Hong Kong, China

<sup>d</sup> Department of Architecture, National University of Singapore, Singapore

<sup>e</sup> Institute of Meteorology and Climatology, Leibniz Universität Hannover, Hannover, Germany

### ARTICLE INFO

#### Article history:

Received 23 August 2016

Received in revised form 16 January 2017

Accepted 4 April 2017

#### Keywords:

Air ventilation assessment (AVA)

Velocity ratio

Urban morphology

High-density city design

Large-eddy simulation (LES)

### ABSTRACT

This study investigates ventilation performance in parametric urban scenarios using a large-eddy simulation (LES) model called the Parallelized LES Model (PALM). With various combinations of planning parameters, air flows and pedestrian-level velocity ratios in a total of 48 scenarios are investigated. Major findings and recommendations are: First, ground coverage ratio ( $\lambda_p$ ) is the most important factor for good ventilation. Second, in cases of homogeneous building heights, a power regression between velocity ratios and aspect ratios of parallel street canyons can be derived, which suggests that good understanding of local microclimate, especially prevailing wind directions in summer, is needed in urban planning. Third, the effects of building height differentials on urban ventilation are connected to urban density. In low-density scenarios, inhomogeneous building heights give worse ventilation performance compared to homogeneous cases. In high-density scenarios, inhomogeneous building heights result in better ventilation performance than homogeneous cases. Inhomogeneous building heights generate more vertical momentum fluxes in street canyons and have a negative (positive) effect on velocity ratios of low-density (high-density) parametric urban fabrics. The application of this point is that homogeneous building heights are recommended when low density is present, and inhomogeneous building heights may be better in cases of high density.

© 2017 Elsevier B.V. All rights reserved.

\* Corresponding author.

E-mail address: [w.wang@cuhk.edu.hk](mailto:w.wang@cuhk.edu.hk) (W. Wang)

<http://dx.doi.org/10.1016/j.uclim.2017.04.007>

2212-0955 © 2017 Elsevier B.V. All rights reserved.

## 1. Introduction

The Fifth Assessment Report of the Intergovernmental Panel on Climate Change (IPCC) has noted that warming of the climate system is unequivocal; 1983–2012 was likely the warmest 30-year period of the last 1400 years in the Northern Hemisphere, and it is likely that the frequency of heat waves has increased in large parts of Europe, Asia, and Australia (IPCC, 2013). Meanwhile, according to the World Health Organization, the urban population in 2014 accounted for 54% of the total global population, up from 34% in 1960, and it continues to grow. The urban heat island effect further intensifies large-scale high temperatures in high-density cities and threatens the inhabitants' health (Wang et al., 2016). In high-density Hong Kong, for example, the rate of warming increased by 0.37 °C per decade between 1989 and 2005, based on the observed temperature (Lam, 2006). The temperature is also projected to rise by 4.4 °C in 2090–2099 for the case of urbanization frozen at its 2006 level, and to rise by 5.2 °C for the case of a constant rate of urbanization (Leung et al., 2007). Mean mortality associated with heat stroke would experience a twofold per unit rise in net effective temperature beyond 26 °C (Leung et al., 2008).

Rapid urbanization in the tropical and subtropical regions means that a better understanding of how to design and plan a city with good ventilation performance is needed. To achieve neutral thermal sensation in an urban environment, a wind speed of 0.9–1.3 m/s is needed for a person wearing light clothing under shaded conditions (Ng and Cheng, 2012). Hence, thermal comfort can be achieved by capturing the natural wind. Meanwhile, good air ventilation is also important for pollutant dispersion in street canyons (Lo and Ngan, 2015; Mirzaei and Haghghat, 2010; Yuan et al., 2014). Outdoor air quality can further affect indoor air quality via natural as well as artificial ventilation, as indoor air will be replaced by outdoor air eventually (Chen, 2009). Therefore, providing good urban air ventilation is very important for quality and healthy living in high-density cities in tropical and subtropical regions (Ng et al., 2011; Yuan and Ng, 2014). However, a distinction should be made between ventilation for air quality and ventilation for thermal comfort. When the purpose is to study ventilation for air quality, the main parameters are flow rate, which provides dilution capacity for contaminants, and turbulent transport at rooftop level, which removes contaminants from street canyons. When the aim is to study ventilation for thermal comfort, the main parameter is wind velocity at the pedestrian level. This study focuses on ventilation for thermal comfort, so the main parameter to be investigated is the wind velocity ratio at the pedestrian level.

Urban ventilation is strongly influenced by wind speed and direction, which in turn are affected by three-dimensional urban morphology (Skote et al., 2005; Yang et al., 2013). As a combination of the individual shapes and dimensions of buildings and their arrangement in the city, urban density can be described by geometric parameters in planning like ground coverage ratio ( $\lambda_p$ ), frontal area density ( $\lambda_f$ ), and plot ratio ( $P$ ). So-called parametric studies, which simplify complex actual urban geometries into simple morphological models, are widely applied in urban ventilation studies for their advantages of linking specific geometric parameters to air ventilation performance. Using a  $\kappa$ - $\omega$  shear stress transport turbulence model, Yuan and Ng (2012) carried out a parametric study with a focus on building porosity for better urban ventilation and evaluated the effects of wind speed on outdoor thermal comfort. Using a standard  $\kappa$ - $\epsilon$  turbulence model, Buccolieri et al. (2015) investigated the breathability in dense building arrays with  $\lambda_p$  values similar to those of typical European cities. Yang and Li (2011) modeled turbulence effects in two simple Hong Kong city models with relatively complex terrain under different atmospheric conditions, and the importance of thermal stratification was highlighted under a weak wind background. Hang et al. (2013) investigated neutral ventilation assessment in two idealized urban models with various approaching wind directions, while Lin et al. (2014) investigated urban canopy layer ventilation under neutral atmospheric conditions with the same  $\lambda_p$  (0.25) and  $\lambda_f$  (0.25) but with various urban sizes, building height variations, overall urban forms, and wind directions. Ramponi et al. (2015) provided a review of the literature for computational fluid dynamics (CFD) studies of outdoor ventilation for generic urban configurations and indicated that there is a lack of studies of urban configurations where not all parallel streets have equal widths. This initiated their CFD simulation of ventilation in generic urban configurations with different urban densities and equal and unequal street widths. Ho et al. (2015) examined flows over idealized two-dimensional street canyons of different building aspect ratios and urban boundary layer depths and utilized the friction factor and the air-exchange rate to parameterize aerodynamic resistance and street-level urban ventilation. Using large-eddy simulation (LES), Nazarian and Kleissl (2016) studied realistic solar heating in a three-dimensional idealized urban environment and investigated mean flow and turbulence statistics as determinants for urban canyon ventilation.

However, comprehensive parametric studies considering a number of varying practical parameters are rarely found in the literature.

Associated with investigations of ventilation in idealized urban models or generic configurations, CFD techniques, such as the Reynolds-averaged Navier-Stokes (RANS) model and LES, are needed. As reviewed above, RANS models have commonly been used in previous CFD studies, mainly due to their low computational cost. However, there is debate regarding the performance of different kinds of RANS models (Hang et al., 2013; Yuan and Ng, 2012). LES overcomes the deficiencies of RANS by explicitly resolving large, energy-containing turbulent eddies and parameterizing only small (subgrid) scale turbulence (Rodi et al., 1997; Tamura, 2008). This advantage of LES comes at a much higher computational cost than RANS. But today's ever-rising computational power makes urban LES applications feasible (Tamura, 2008). The dimensionality, spatial resolution, and turbulence intensity that an LES model can handle are superior to those of most other methodologies (Castillo et al., 2011). What affects pedestrian comfort directly is the wind flow within cities, and the local turbulence level in particular (Britter and Hanna, 2003). LES provides not only mean flow fields but also instantaneous turbulences, which are especially important for human comfort at the pedestrian level in the urban canopy layer. We therefore use an LES model to produce CFD simulations of air flow and ventilation performance in a set of comprehensive parametric urban scenarios in this study.

## 2. The Parallelized LES Model (PALM)

The LES model used in this study is the Parallelized LES Model (PALM), which was developed in 1997 (Raasch and Schröter, 2001), when it was one of the first parallelized LES models for atmospheric research (Maronga et al., 2015). The governing equations of PALM are based on the non-hydrostatic, filtered, incompressible Navier-Stokes equations with Boussinesq approximation and are filtered implicitly using the volume-balance approach of Schumann (Schumann, 1975). The first law of thermodynamics and an equation for subgrid-scale turbulent kinetic energy are used in the basic model. The Monin-Obukhov similarity theory is applied between the surface and the first grid level. A Prandtl layer is assumed at each surface. The modified version (Moeng and Wyngaard, 1988; Saiki et al., 2000) of the 1.5-order Deardorff scheme (Deardorff, 1980) is used for turbulence closure. The Temperton algorithm (Temperton, 1992) for the fast Fourier transform is used to solve for the Poisson equation for the perturbation pressure. For the time integration, a third-order Runge-Kutta scheme (Williamson, 1980) is used. The advection scheme used is the second-order scheme of Piacsek and Williams (Piacsek and Williams, 1970). Alternatively, a fifth-order scheme developed by Wicker and Skamarock (Wicker and Skamarock, 2002) can be utilized. PALM has been validated for simulating flows and turbulence characteristics at the street-canyon and neighbourhood scale (Letzel et al., 2008) and has been widely used in studies of urban street-canyon flows in recent years (Inagaki et al., 2011; Kanda et al., 2013; Keck et al., 2014; Letzel et al., 2012; Park and Baik, 2014; Park et al., 2012). The code used in this study is PALM version 4.0 (Maronga et al., 2015).

### 2.1. Output indicator and simulation setup

In air ventilation assessment (AVA) studies, we are especially interested in pedestrian-level wind velocity. The wind velocity ratio is used as an indicator. It is calculated by  $V_p/V_\infty$ , where  $V_p$  is the wind velocity at the pedestrian level (2 m above ground), and  $V_\infty$  is the wind velocity at the top of the wind boundary layer not affected by ground roughness. In both  $V_p$  and  $V_\infty$ , only horizontal velocity components are taken into account. A commonly used top boundary layer height of 500 m in CFD and wind tunnel tests of AVA (Ng, 2009) is adopted in this study. Winds are assumed to come from the left in all LES experiments, as the calculation of frontal area density  $\lambda_f$ , which will be discussed later, is also based on this assumption. A wind speed of 1.5 m/s is prescribed.

Horizontal grid sizes are equidistantly 2 m. The vertical grid spacing is 2 m below 300 m and stretched with a stretch factor of 1.04 above. The governing equations of PALM are spatially discretized on an Arakawa-C grid (Arakawa and Lamb, 1977; Harlow and Welch, 1965). Scalar variables are defined at the grid centers, while velocity components are shifted by half of the grid spacing. Therefore, horizontal velocity output from the 1 m and 3 m levels is linearly interpolated to obtain  $V_p$  at 2 m above the ground. The total simulation time is 6 h. The first 4 h are excluded in the analysis of the results, as the turbulences need this time to spin-up (Letzel et al., 2008). The simulated results from the 5th to the 6th hours are averaged for analysis. Cyclic

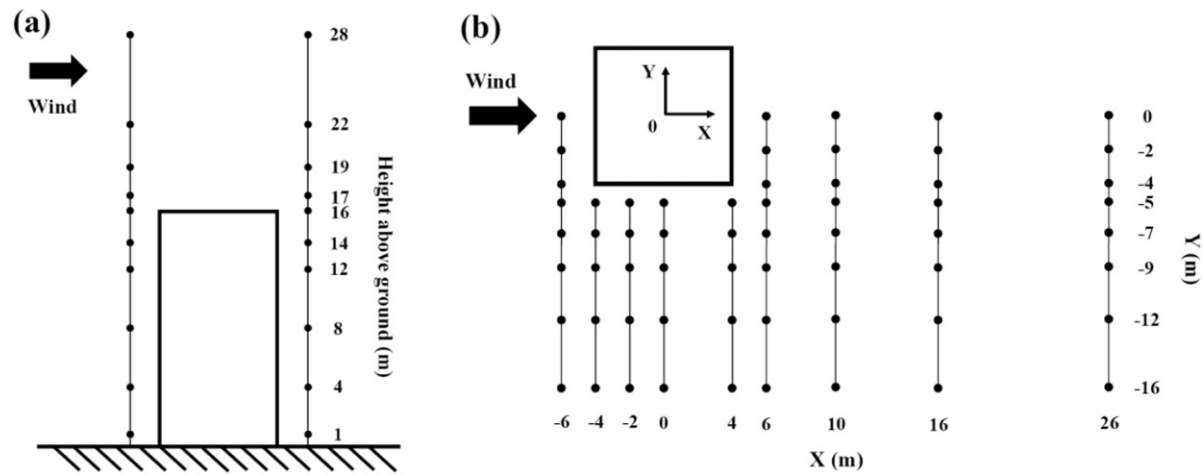


**Fig. 1.** Locations of test points in the Architectural Institute of Japan (AIJ) guidelines setup for a single building: (a) Lateral view of the two profiles and 20 test points taken at 2 m away from the building to windward and leeward. (b) Aerial view of 60 horizontal test points around the building at 1 m above the ground. This figure is adopted and modified from the AIJ guidelines ([http://www.aij.or.jp/jpn/publish/cfdguide/index\\_e.htm](http://www.aij.or.jp/jpn/publish/cfdguide/index_e.htm)).

(periodic) boundary conditions are adopted in both the streamwise and spanwise directions. The no-slip bottom boundary condition with a Prandtl layer and the free-slip top boundary condition are applied to horizontal velocity components. The simulations are restricted to neutral atmospheric stratification, i.e., thermal effects are not considered.

## 2.2. Model validation

We use the CFD guidelines proposed by a working group from the Architectural Institute of Japan (AIJ) to verify the PALM codes. The AIJ guidelines are based on the results of cross-comparisons of CFD predictions, wind tunnel tests, and field measurements (Tominaga et al., 2008). We conducted LES experiments with the 2:1:1 shape building model as well as simple building blocks that comply with AIJ guidelines. The CFD setups and experimental data for verification can be found on the AIJ website ([www.aij.or.jp/jpn/publish/cfdguide/index\\_e.htm](http://www.aij.or.jp/jpn/publish/cfdguide/index_e.htm)). Details for the single-building case can be found in Mochida et al. (2002), while introductions of all seven test cases can be found in Tominaga et al. (2008).

For the single-building case, the horizontal computational domain size is  $172 \text{ m} \times 108 \text{ m}$ . An equidistant horizontal grid size of 0.5 m is used. In the vertical direction, a grid size of 0.5 m is adopted below 24 m and a stretch with a stretch factor of 1.05 is applied above. With 90 vertical levels, the domain height is about 100 m. The building height is 16 m. It is noteworthy that for this simulation of a single building, a noncyclic boundary condition in the streamwise direction is adopted. Otherwise, it will become a simulation of an infinite row of buildings. Validation is accomplished by comparing PALM-computed results and AIJ guidelines in terms of wind profiles around the building and wind velocity taken from near-surface test points. Fig. 1a shows the profiles at 2 m away from the single building to windward and leeward, while Fig. 1b shows the locations of 60 test points at 1 m above the ground.

The inlet mean wind profile in the PALM experiment is the same as that given in the guidelines, as shown in the black profile in Fig. 2a. Fig. 2a compares velocity profiles at 2 m away from the single building to windward (red lines) and leeward (blue lines). Dashed lines represent AIJ referential data, while solid lines indicate results predicted by PALM. Stronger rooftop vortex and velocity fluctuation compared to AIJ data can be observed in Fig. 2a, but overall good agreement between the two suggests that PALM can capture the wind profile features around the building. As this study focuses on pedestrian-level ventilation, the computational performance of PALM in reproducing near-surface velocity may be more important. Fig. 2b is a scatter plot of PALM-computed velocity and AIJ experimental data at 60 test points. The comparison in Fig. 2b gives

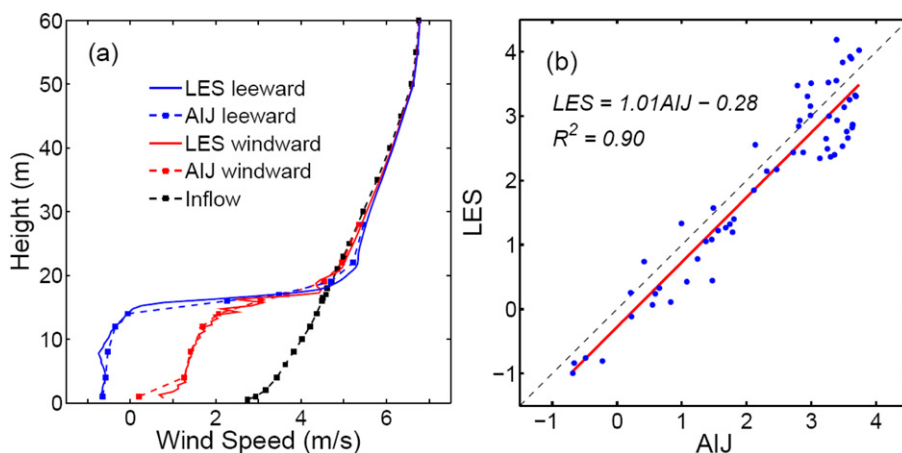


**Fig. 2.** Cross-comparison between Architectural Institute of Japan (AIJ) experimental data and PALM results: (a) Vertical wind profiles in the windward (red lines) and leeward (blue lines) position at 2 m from the building; the inflow is shown by the black profile. (b) Linear regression between AIJ and PALM results in the test points at 1 m above the ground.

substantial confidence to using PALM to study pedestrian-level wind flow, as all points are located close to the diagonal line. A linear regression with an  $R^2$  of 0.9 can be obtained.

Validation for simulation of air flow around only a single building may not be convincing for this study. For validation cases with simple building blocks, the building arrays, inlet mean wind profile, and locations of test points are shown in Fig. 3. The experiments include 9 buildings with a uniform building height of  $H = 20$  m, except the one in the middle, which is prescribed a varying building height for each case of 0H, 1H, and 2H, respectively (Fig. 3a). The buildings are horizontally foursquare and both the buildings and the streets are 20 m wide. In the PALM experiments, the computational domain size is  $300 \text{ m} \times 200 \text{ m} \times 120 \text{ m}$ . An equidistant grid size of 0.5 m is used both horizontally and vertically. The inlet mean wind profile is the same as that given in the guidelines and shown in Fig. 3b. Velocity values taken from 120 test points at 2 m above the ground are used to validate the PALM simulation. The test point locations are shown in Fig. 3c (black dots).

The validation results are shown in Fig. 4. Generally, the scatter dots are located close to the diagonal lines, but the results predicted by PALM may have slightly underestimated the near-surface velocity compared to AIJ guidelines, particularly in those test points with relatively low wind speed. A linear regression with an  $R^2$  of 0.82, 0.77, and 0.60 can be obtained for cases 0H, 1H, and 2H, respectively. The complex level of the building arrays may affect the accuracy of the PALM prediction. But in general, no significant deviations are found in the above validations. The PALM model is therefore deemed to be a suitable LES tool for this study.

### 3. Parametric urban scenarios

Parametric scenarios of generic urban configurations are defined in a practical way. Building dimensions and street layouts are calculated from practical geometric parameters for urban planning. Nomenclature of all involved parameters and their values is given in Table 1. The first three parameters are to be investigated and their values are prescribed in Table 2. The plot ratio  $P$  is obtained by dividing the gross floor area of the building by the area of the site on which the building is erected (site area,  $S$ ). For instance, if a building has 10 storeys and the area of each floor is  $800 \text{ m}^2$ , then the gross floor area is  $8000 \text{ m}^2$ . If the site area is  $1000 \text{ m}^2$ , the plot ratio  $P$  is 8. The ground coverage ratio  $\lambda_p$ , which is also called packing density, building area density, or plan area ratio, is the ratio of ground area that is covered by the building to the site area. The frontal area density  $\lambda_f$  is the ratio of building frontal area that faces the wind blowing into the site area. To give finite solutions, the site area ( $S$ ) is assumed to be  $1 \text{ km}^2$ , the floor height ( $h$ ) is assumed to be 3 m, and the floor area ( $A$ ) is assumed to be approximately  $2000 \text{ m}^2$  or  $4000 \text{ m}^2$ , depending on the value of the plot ratio ( $P$ ). If  $P = 3$ , a residential building and floor area of about  $2000 \text{ m}^2$  is assumed, while if  $P = 8$ , a commercial building and floor area of about  $4000 \text{ m}^2$  is assumed. In the case of  $P = 5$ , it can be either a residential or commercial building, and the floor area depends on the combination of  $P$  and  $\lambda_f$ . A floor area of about  $4000 \text{ m}^2$  gives a more realistic building length-to-width aspect in the case of  $\lambda_f = 0.1$ , while in the case of  $\lambda_f = 0.25$  or  $0.4$ , a floor area of about  $2000 \text{ m}^2$  is assumed.

Given the prescribed and assumed parameters in Tables 1 and 2, other geometric parameters in Table 1 can be calculated as follows:

Building height ( $H$ ):

$$H = hP/\lambda_p \quad (1)$$

Building number ( $N$ ):

$$N = S\lambda_p/A \quad (2)$$

Building size (frontal size  $L$ ):

$$L = A\lambda_f/hP \quad (3)$$

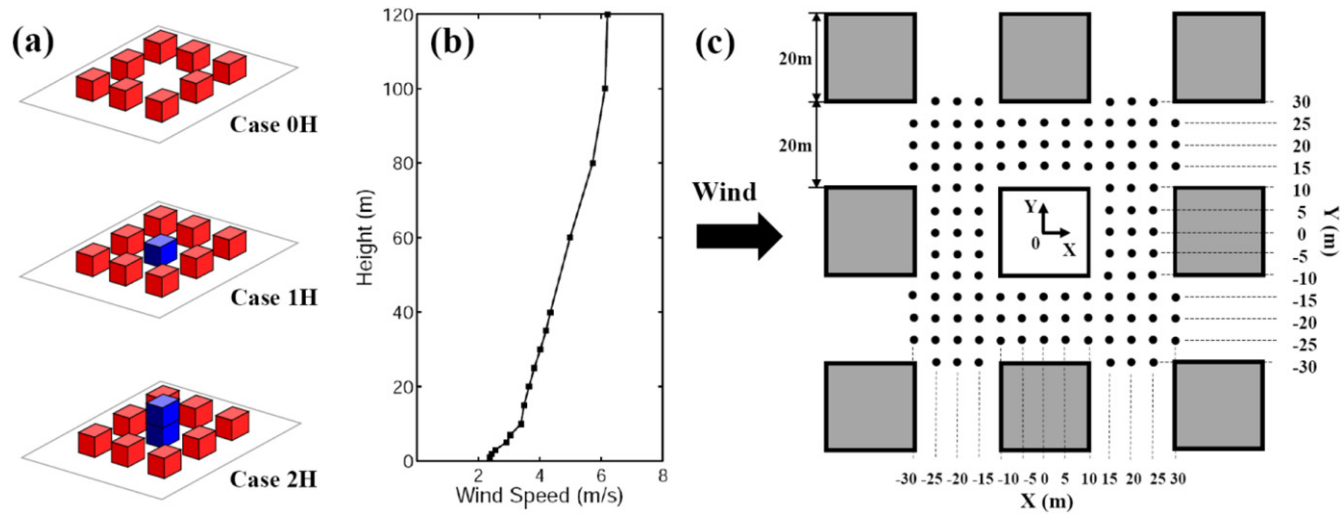


**Fig. 3.** Setups of validation cases for simple building blocks: (a) Building arrays of three cases, (b) The inlet mean wind profile, and (c) Building geometries (boxes) and locations of test points (black dots). This figure is adopted and modified from the AIJ guidelines ([http://www.aij.or.jp/jpn/publish/cfdguide/index\\_e.htm](http://www.aij.or.jp/jpn/publish/cfdguide/index_e.htm)).

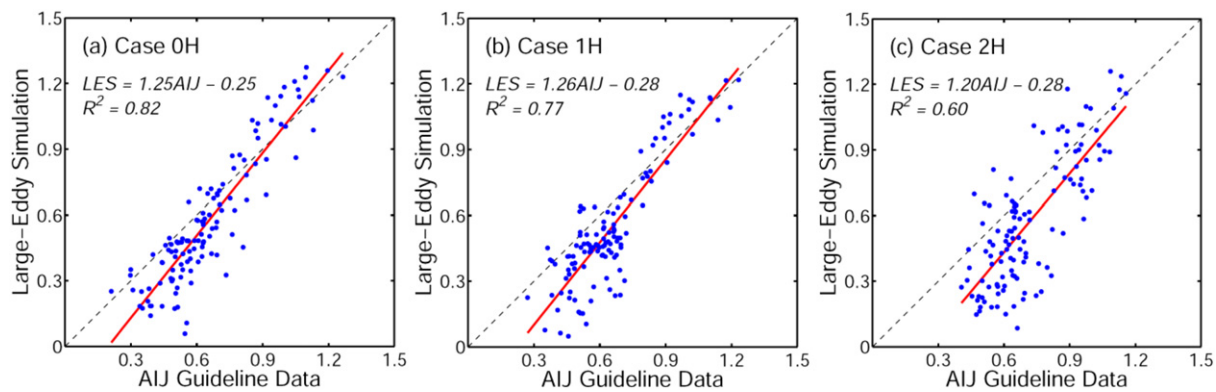


**Fig. 4.** Linear regression between referential velocity of Architectural Institute of Japan (AIJ) guidelines and large-eddy simulation (LES) results taken from 120 test points at 2 m above the ground in simple building blocks for (a) Case 0H, (b) Case 1H, and (c) Case 2H.

**Table 1**  
Nomenclature of involved parameters and values.

Parameters and nomenclature		Value(s)
P	Plot ratio	Variable prescribed in Table 2
$\lambda_f$	Frontal area density	Variable prescribed in Table 2
$\lambda_p$	Ground coverage ratio	Variable prescribed in Table 2
S	Site area	Assumed to be 1 km <sup>2</sup>
h	Floor height	Assumed to be 3 m
A	Floor area	Approximated at 2000 m <sup>2</sup> or 4000 m <sup>2</sup> ; depends on P
H	Building height	Calculated by Eq. (1), in meters
N	Building number	Calculated by Eq. (2)
L	Frontal building size	Calculated by Eq. (3), in meters
D	Perpendicular building size	Calculated by Eq. (4), in meters
R	Building matrix: row	Maximized theoretical N in the given S
C	Building matrix: column	Maximized theoretical N in the given S
$W_S$	Parallel street width	Calculated by Eq. (5), in meters
$W_S'$	Perpendicular street width	Calculated by Eq. (6), in meters

Building size (perpendicular size D):

$$D = hP/\lambda_f \quad (4)$$

In addition, row and column numbers of the building matrix have to be fitted to the 1-km<sup>2</sup> site area. Perpendicular and parallel street widths are herein obtained.

Street width (parallel width  $W_S$ ):

$$W_S = (1000 - LR)/R \quad (5)$$

Street width (perpendicular width  $W_S'$ ):

$$W_S' = (1000 - DC)/C \quad (6)$$

The schematic diagram in Fig. 5 elucidates the meanings of the involved geometric parameters. All values computed from Eqs. (3)–(6) are coerced to the closest even-integral numbers, as the horizontal resolution in the PALM setup is 2 m. Therefore, the actual values of the prescribed variables may differ slightly from the original values in Table 2. From all combinations of variables given in Table 2, a total of 27 scenarios with homogeneous (HM) building heights can be obtained, but the ratio of building size (frontal size L and perpendicular size D) should not be too large in order to be realistic. A combination of  $P = 8$  and  $\lambda_f = 0.1$  will result in unrealistically long buildings. Therefore, a total of 24 scenarios for homogeneous building heights are chosen. The results are listed in Table 3. For inhomogeneous (IM) scenarios, building heights are generated by a normally distributed random series, which is given a mean of the corresponding homogeneous building height (H) and a standard deviation of H/4. According to the tolerance intervals of normal distribution, a standard deviation of H/4 can basically (99.99%) ensure that no negative random building heights will be generated. Fig. 6 shows two examples of homogeneous and corresponding inhomogeneous building heights in a lateral view. Moreover, to avoid wind blowing directly into street canyons, normalized blocks with sizes of 40 m × 40 m × 10 m are set around every model. The block height is 10 m so as to be lower than the smallest building height of 12 m in the parametric scenarios (Table 3). As the site area S is assumed to be 1 km<sup>2</sup>, the actual computational domain is 1.2 km × 1.2 km.

**Table 2**  
Prescribed values of 4 parameters for defining 48 parametric scenarios.

Parameters to be investigated	Given values		
Plot ratio (P)	3	5	8
Frontal area density ( $\lambda_f$ )	0.1	0.25	0.4
Ground coverage ratio ( $\lambda_p$ )	25%	50%	75%
Height differential	homogeneous	inhomogeneous	

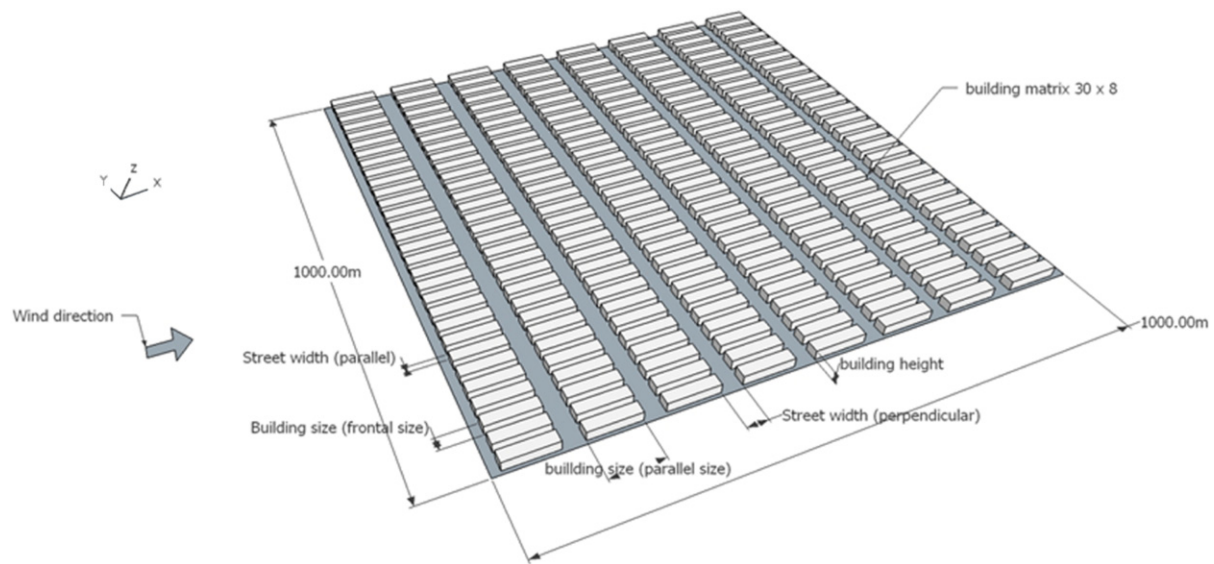


Fig. 5. Schematic diagram showing definitions of geometric parameters.

**Table 3**  
Parametric scenarios of various urban morphologies and PALM-computed site-averaged velocity ratios.

Scenario ID	Plot ratio (P)	Frontal area density ( $\lambda_f$ )	Ground coverage ratio ( $\lambda_p$ )	Floor area (A)	Building number (N)	Building matrix: row (R)	Building matrix: column (C)	Building height (H)	Frontal building size (L)	Perpendicular building size (D)	Parallel street width (W)	Perpendicular street width (W')	Aspect ratio (H/W)	Velocity ratio of HM	Velocity ratio of IM
HM&IM01	3.0	0.1	25%	2160	120	12	10	36	24	90	60	10	0.60	0.196	0.147
HM&IM02	3.0	0.1	50%	2160	232	29	8	18	24	90	10	34	1.80	0.073	0.090
HM&IM03	3.0	0.1	75%	2160	330	33	10	12	24	90	6	10	2.00	0.050	0.058
HM&IM04	3.0	0.25	25%	2128	121	11	11	36	56	38	34	52	1.06	0.098	0.118
HM&IM05	3.0	0.25	50%	2128	240	15	16	18	56	38	10	24	1.80	0.083	0.092
HM&IM06	3.0	0.25	75%	2128	336	16	21	12	56	38	6	8	2.00	0.036	0.065
HM&IM07	3.0	0.4	25%	2160	120	10	12	36	90	24	10	60	3.60	0.109	0.142
HM&IM08	3.0	0.4	50%	2160	232	8	29	18	90	24	36	10	0.50	0.128	0.105
HM&IM09	3.0	0.4	75%	2160	330	10	33	12	90	24	10	6	1.20	0.057	0.064
HM&IM10	5.0	0.1	25%	4200	60	12	5	60	28	150	56	50	1.07	0.138	0.124
HM&IM11	5.0	0.1	50%	4200	120	20	6	30	28	150	22	16	1.36	0.130	0.104
HM&IM12	5.0	0.1	75%	4200	174	29	6	20	28	150	6	16	3.33	0.036	0.075
HM&IM13	5.0	0.25	25%	2160	121	11	11	60	36	60	54	30	1.11	0.130	0.094
HM&IM14	5.0	0.25	50%	2160	240	16	15	30	36	60	26	6	1.15	0.149	0.093
HM&IM15	5.0	0.25	75%	2160	330	22	15	20	36	60	8	6	2.50	0.059	0.066
HM&IM16	5.0	0.4	25%	2160	120	10	12	60	54	40	46	44	1.30	0.084	0.095
HM&IM17	5.0	0.4	50%	2160	225	15	15	30	54	40	12	26	2.50	0.059	0.096
HM&IM18	5.0	0.4	75%	2160	352	16	22	20	54	40	8	6	2.50	0.049	0.071
HM&IM19	8.0	0.25	25%	4032	63	9	7	96	42	96	70	46	1.37	0.132	0.097
HM&IM20	8.0	0.25	50%	4032	126	18	7	48	42	96	14	46	3.43	0.061	0.102
HM&IM21	8.0	0.25	75%	4032	180	20	9	32	42	96	6	16	5.33	0.025	0.080
HM&IM22	8.0	0.4	25%	3960	63	7	9	96	66	60	76	52	1.26	0.096	0.097
HM&IM23	8.0	0.4	50%	3960	121	11	11	48	66	60	24	30	2.00	0.079	0.098
HM&IM24	8.0	0.4	75%	3960	182	13	14	32	66	60	10	11	3.20	0.049	0.084

### 4. Results and discussion

#### 4.1. Identification of the most important factor

Taking scenarios HM/IM01 and HM/IM04 as examples, Fig. 6 shows the vertical distributions of streamwise horizontal velocity and some general flow features in the main runs. Frontal views of streamwise velocity in a y-z section are shown for HM01 (Fig. 6a) and IM01 (Fig. 6b). Differential canopy heights in the spanwise direction are found. Lateral views of streamwise velocity in an x-z section are shown for HM04 (Fig. 6c) and IM04 (Fig. 6d). Velocity rotations behind buildings are prominent, which suggests that a “skimming” flow regime or a “wake interference” flow regime, rather than an “isolated roughness” flow regime, is dominant in this scenario (Hunter et al., 1992; Oke, 1988). The overall results suggest that the aforementioned

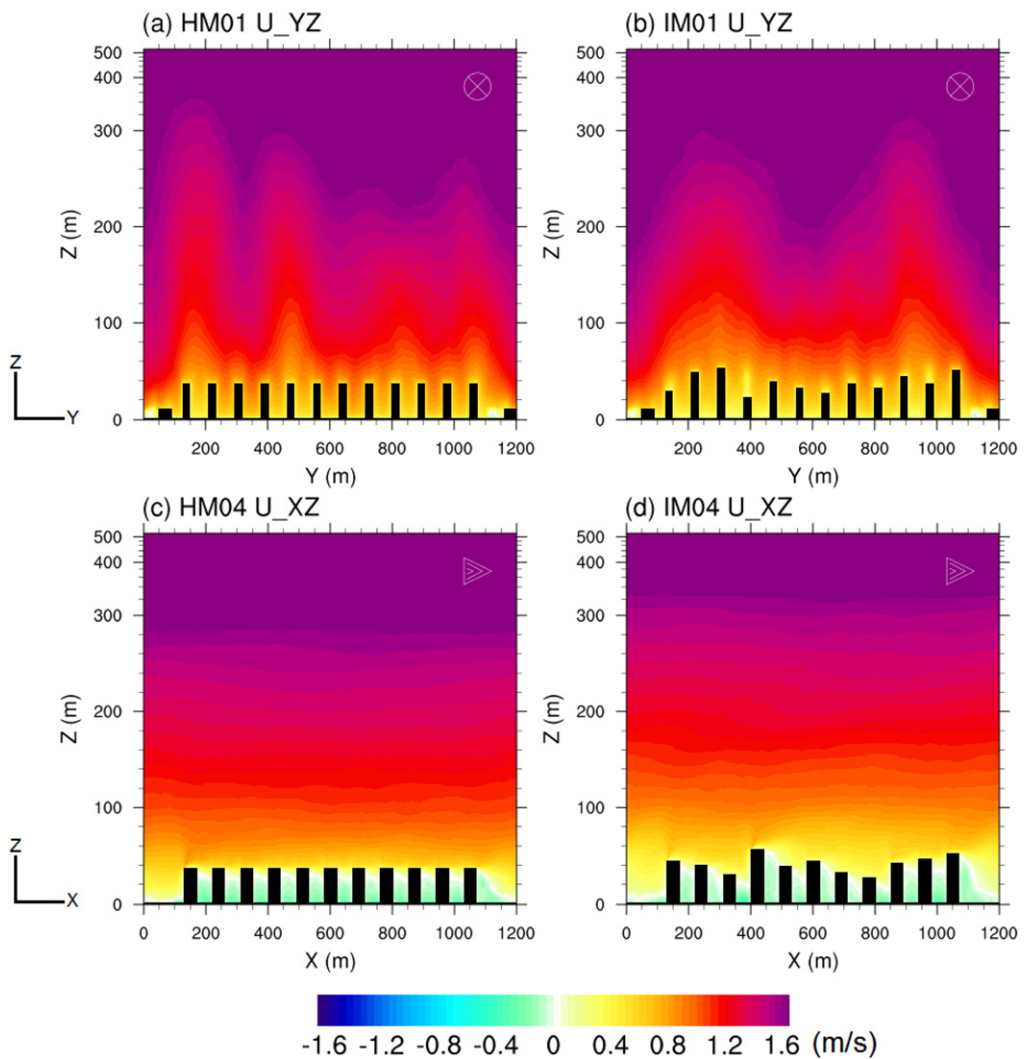


Fig. 6. Vertical sections of streamwise horizontal velocity in (a) HM01, (b) IM01, (c) HM04, and (d) IM04. Black boxes at the bottom denote buildings. Symbols in the upper right corner indicate wind direction.

top level of 500 m is high enough to capture the whole canopy layer, as the reduced velocity layer (canopy layer) cannot reach the top level of 500 m height, and this is also found in other scenarios (not shown).

This study focuses on pedestrian-level ventilation. Velocity ratios of all 48 scenarios are shown in Fig. 7 (homogeneous scenarios) and Fig. 8 (inhomogeneous scenarios). Building heights can be identified by the grey colour scale. We further select an assessment area 200 m away from the lateral boundary in all horizontal directions, that is, an 800 m  $\times$  800 m domain in the middle of all parametric models. This satisfies the AVA requirement of a buffer width of at least one building height of the tallest building on site. More importantly, this avoids the uncertainty caused by the numerical lateral boundary conditions, as can be seen in Figs. 7 and 8. For example, the obviously higher velocity ratios near the streamwise windward boundaries in most cases are excluded, and the higher velocity ratios near the spanwise boundaries in HM07 (Fig. 7g) are excluded as well.

Figs. 7 and 8 demonstrate spatial patterns and details, but to quantify the effects of planning parameters on ventilation performance, we first analyze PALM-computed velocity ratios in terms of site-averaged values in the assessment area, which are listed in the last two columns of Table 3. These site-averaged velocity ratios are classified into groups regarding different values of the prescribed parameters (Fig. 9). In Fig. 9a,  $P$  and  $\lambda_f$  are

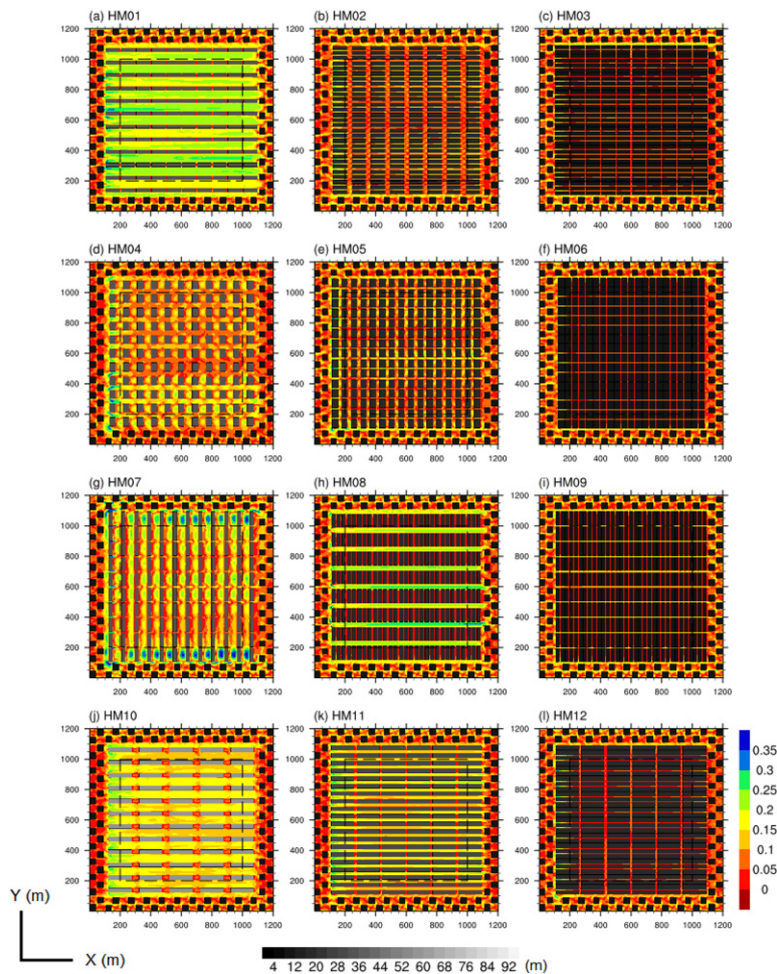


Fig. 7. Spatial distributions of time-averaged velocity ratios in homogeneous parametric scenarios. The rainbow (vertical) colour bar is for velocity ratios, and the grey (horizontal) colour bar is for building heights. Dashed boxes denote the assessment areas.

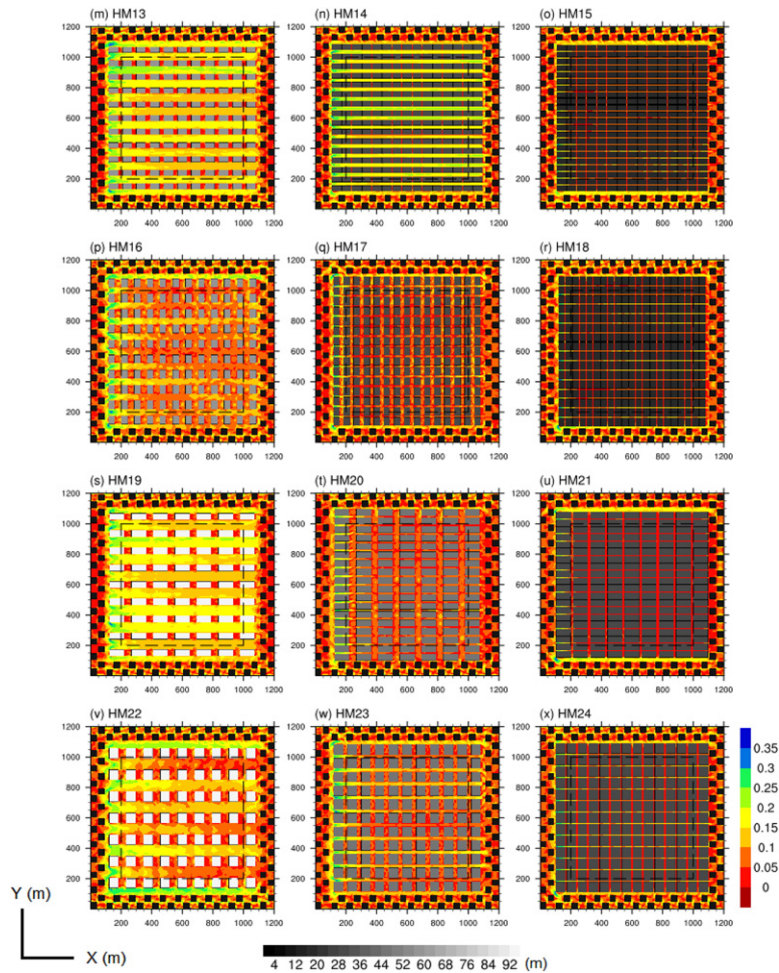


Fig. 7 (continued)

fixed inside one group, while  $\lambda_p$  is changing, Group No.1 is HM01–03, Group No.2 is HM04–06, etc. Fig. 9b is the same as Fig. 9a but for inhomogeneous parametric scenarios. Hence, Fig. 9a–b shows the results of all 48 simulations. These are repeated in Fig. 9c–d with fixed  $P$  and  $\lambda_p$ , with changing  $\lambda_f$ . In Fig. 9c (d), Group No.1 is HM (IM) 01, 04, and 07, Group No. 2 is HM (IM) 02, 05, and 08, etc. Group Nos. 7–9 have only two bars, as no combination of  $P = 3$  and  $\lambda_f = 0.1$  are modeled. All 48 results are repeated again in Fig. 9e–f with fixed  $\lambda_f$  and  $\lambda_p$ , with changing  $P$ . In Fig. 9e (f), Group No.1 is HM (IM) 01 and 10, Group No. 2 is HM (IM) 02 and 11, etc.

Grouped in this way, the most important parameter for pedestrian-level ventilation performance can be identified. As can be seen from Fig. 9a, a lower  $\lambda_p$  will generally result in a higher site-averaged velocity ratio. There are two exceptions, Group Nos. 3 and 5, in which site-averaged velocity ratios are slightly higher when  $\lambda_p = 0.5$  than when  $\lambda_p = 0.25$ ; that is, the site-averaged velocity ratio of HM08 (0.128) is higher than that of HM07 (0.109), and that of HM14 (0.149) is higher than that of HM13 (0.130). A potential cause for these exceptions is the building height. Homogeneous scenario HM08 with  $H = 18$  m gives a higher velocity ratio compared to HM07 with  $H = 36$  m, and HM14 with  $H = 30$  m has better ventilation performance than HM13 with  $H = 60$  m. The effects of building heights and their differentials will be further discussed in the following sections. For scenarios of inhomogeneous building height, the effect of  $\lambda_p$  is also essential (Fig. 9d). The site-averaged velocity ratios in cases of  $\lambda_p = 0.25$  and  $0.5$  in Group Nos. 5–8 in Fig. 9d are

very close. They are IM13 and 14, IM16 and 17, IM19 and 20, and IM22 and 23. From Table 3 and Fig. 8, we can suggest that a possible cause of what makes the velocity ratios in cases of  $\lambda_p = 0.5$  close to those in cases of  $\lambda_p = 0.25$  is again the building heights and their differentials. When it comes to the other two groupings in Fig. 9, it is difficult to identify a substantial effect on the pedestrian-level velocity ratio when the focus is on the single parameter  $P$  or  $\lambda_f$ . In Fig. 9b, for example, only one group (Group No. 4, with  $P = 5$  and  $\lambda_p = 25\%$ ) conforms to the idea that lower  $\lambda_f$  gives better ventilation performance. In Group No. 2, with  $P = 5$  and  $\lambda_p = 50\%$ , lower  $\lambda_f$  gives even worse ventilation performance. Therefore, the ground coverage ratio  $\lambda_p$  is identified as the most important factor for ventilation performance.

To statistically capture the spatial differences in the velocity ratios given in Figs. 7 and 8, the distributions of these ratios taken from random test points are shown in Fig. 10. In this analytical procedure, all street (non-built) grid points inside the assessment area (200 m away from the lateral boundary in all horizontal directions, as shown in the dashed boxes in Figs. 7 and 8) in each scenario are stored in a 1-D array, and 1000 test points are randomly taken from each array. The random function calculates the interval between test points using a normal distribution with a mean of the array size divided by the number of test points (1000) and a standard deviation of 25% of the mean; thus the test points are randomly spread throughout the whole assessment area. Furthermore, sensitivity tests were conducted regarding the number of test

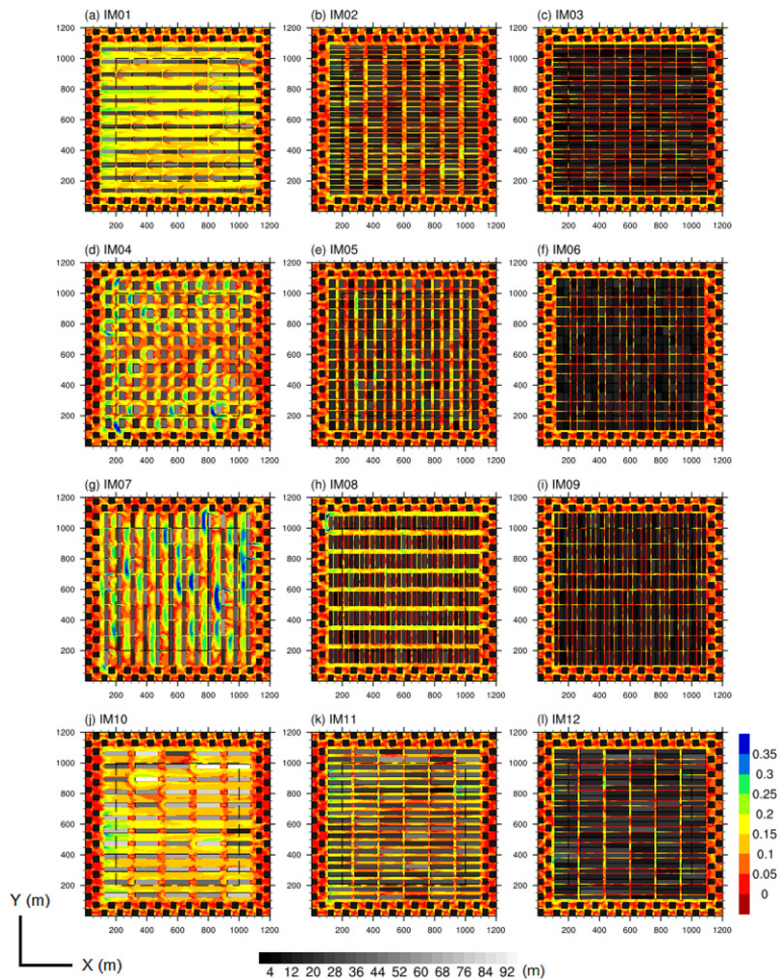


Fig. 8. Same as Fig. 7 but for inhomogeneous parametric scenarios.

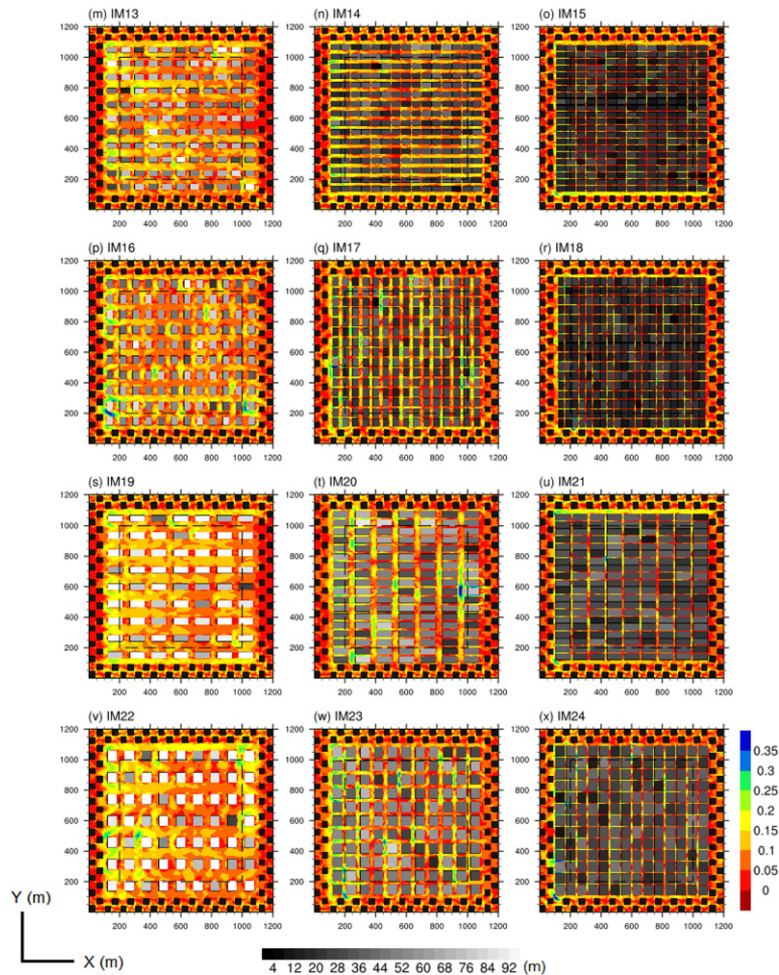
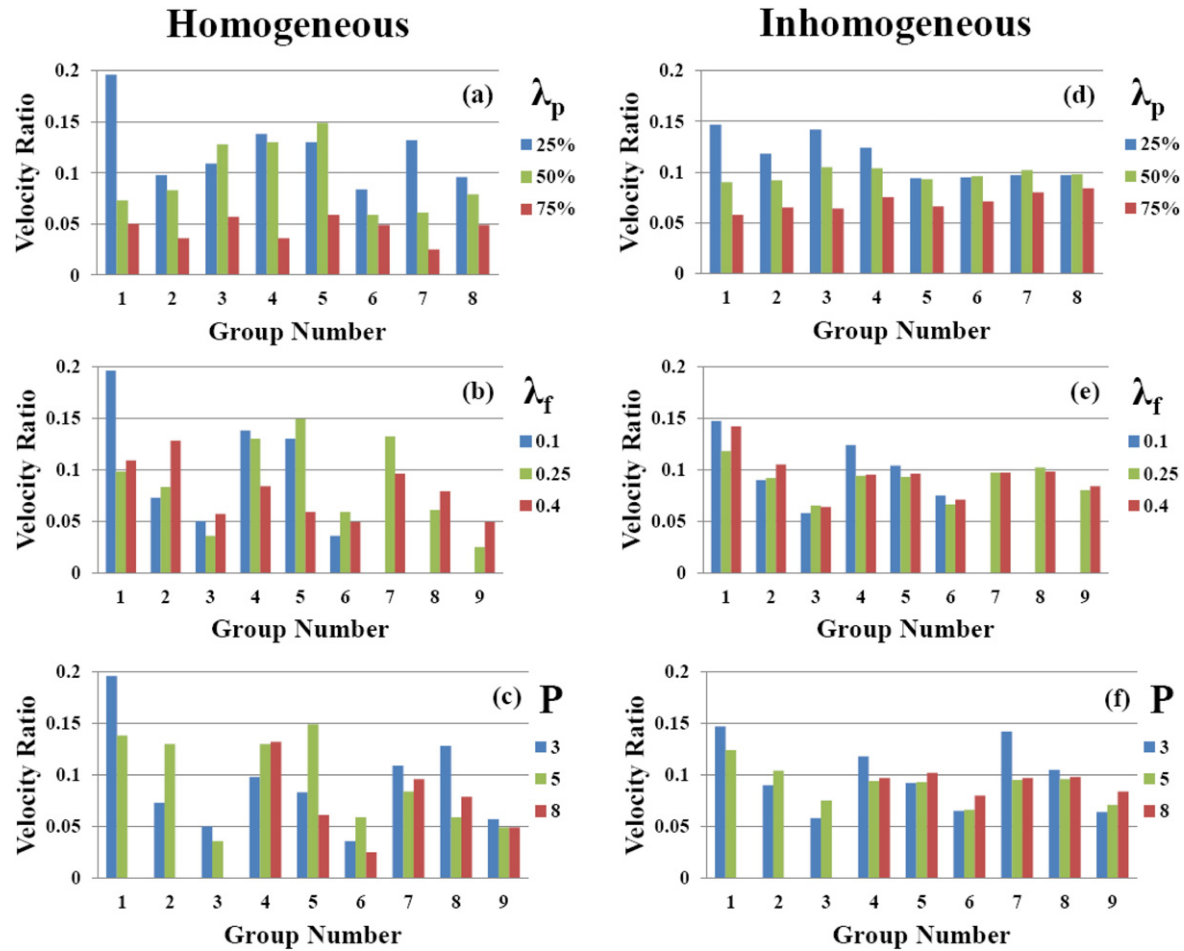


Fig. 8 (continued)

points, and no significant differences were found when the number of test points was larger than 200, which means that any sample number above 200 would be enough to produce the distributions in Fig. 10.

In each panel of Fig. 10, the plot ratio  $P$  and frontal area density  $\lambda_f$  are fixed. Different lines represent changes in  $\lambda_p$  as well as building height differential. Velocity ratio distributions of parametric models with  $\lambda_p = 0.25$  are shown in blue,  $\lambda_p = 0.5$  are shown in green, and  $\lambda_p = 0.75$  are shown in red. Homogeneous scenarios are given in solid lines, while inhomogeneous scenarios are given in dashed lines. Fig. 10 further demonstrates the significance of  $\lambda_p$  in affecting the performance of pedestrian-level ventilation. In most cases, blue lines give the best ventilation performance compared with the other two, while red lines are generally the worst. This is the case for both homogeneous (solid lines) and inhomogeneous (dashed lines) parametric scenarios. A few exceptions can be found, which are consistent with the results presented in Fig. 9a and b.

The significance of  $\lambda_p$  and  $\lambda_f$  for urban ventilation have been widely examined in previous studies, as reviewed in the introduction. But a real city or urban area has complex characteristics and is difficult to model using just a few idealized and simplified parameters. Meanwhile, in-city air flows are very sensitive to building geometries and urban morphologies. The conclusion we derived above from Figs. 9 and 10 may be sensitive to the prescribed values in Table 2. Anyhow,  $\lambda_p$  is more simply defined and directly related to



**Fig. 9.** Bar charts of grouped site-averaged velocity ratio: (a, d) fixed plot ratio ( $P$ ) and frontal area density ( $\lambda_f$ ) with changing ground cover ratio ( $\lambda_p$ ), (b, e) fixed  $P$  and  $\lambda_p$  with changing  $\lambda_f$ , and (c, f) fixed  $\lambda_f$  and  $\lambda_p$  with changing  $P$  for homogeneous models. Homogeneous scenarios are shown in a–c, and inhomogeneous scenarios are shown in d–f.

the term “urban density” compared to the other parameters. Based on this fact, the combined effects of the other parameters are of further interest.

#### 4.2. Aspect ratio of street canyons and combined effects

We have concluded that the most important factor in ventilation performance is the ground coverage ratio  $\lambda_p$ . But exceptions are identified as well, which implies that the effects of other parameters cannot be ignored. More importantly, all geometric parameters are related to each other through Eqs. (1)–(6). In Fig. 7, one may deduce that a higher velocity ratio can be obtained with a wider street that is parallel to the inlet wind direction. But in some cases, building height also plays an important role. For example, the velocity ratios (both the site-averaged value and the distribution of values taken from random test points) in HM11 are very close to those in HM10, though the former has a  $\lambda_p$  value twice as large as the latter (Fig. 10d). The ventilation performance of HM14 is even better than that of HM13 (Fig. 10e), as discussed above. Therefore, the importance of aspect (building height to street width) ratios should be examined.

In Fig. 11a, a scatter plot (blue dots) between the site-averaged velocity ratio and the aspect ratio of the street canyon parallel to the inlet wind direction is given. The aspect ratios of parallel streets, which are derived from the homogeneous building heights and the parallel street widths, are listed in Table 3 as well. A regression model between these two variables can thereby be derived. A power regression in the form of

$$f(x) = c_1 x^{c_2} + c_3 \quad (7)$$

is found to best fit, where  $x$  stands for parallel aspect ratios, and  $f(x)$  represents velocity ratios. The coefficients  $c_1$ ,  $c_2$ , and  $c_3$  decide the regression. For the site-averaged velocity ratio, 0.23,  $-0.28$ , and  $-0.11$  can be obtained for  $c_1$ ,  $c_2$ , and  $c_3$ , respectively (the red line in Fig. 11a). Herein, the coefficient  $c_1$  is positive, while  $c_2$  is negative, which suggests a negative correlation between parallel aspect ratios and velocity ratios. The power regression model further implies a significant influence of aspect ratio on urban ventilation compared with a linear regression model. The  $R^2$  is 0.58 for the current fitting. An evident outlier is HM07, which has a high parallel aspect ratio of 3.6 and a site-averaged velocity ratio of 0.109. This is mainly because of a combination of relatively low  $\lambda_p$  (0.25) but high  $\lambda_f$  (0.4) in HM07, which results in a narrow parallel street of 10 m, but a wide perpendicular street of 60 m (Table 3); hence relatively good ventilation can be obtained with a high parallel aspect ratio.

To further examine Eq. (7) with more samples, we apply the power regression to velocity ratios of random test points. Two hundred test points are randomly taken from the parallel street canyons with crossings excluded in each homogeneous scenario. The scattered points are plotted with blue dots in Fig. 11b. As one may expect, the regression coefficients change slightly compared to the results of site-averaged velocity ratios. As noted in Fig. 11b,  $c_1$ ,  $c_2$ , and  $c_3$  are 0.33,  $-0.28$ , and  $-0.18$ , respectively. But the power regression is still valid as before, with an  $R^2$  of 0.60.

The samples (scatter points) for the regressions in Fig. 11 are rather scattered, which may be owing to the limitation of such a parametric study. That is, we can simulate only a few values for each parameter (Table 2); adding one value to every single parameter would require substantial additional LES experiments and computational capacity. But we think this power regression still has some meaning, or at least it is more representative than a linear relation. Using wind tunnel experiments and field measurements, a previous study suggested a linear correlation between the velocity ratio and  $\lambda_p$  (Yoshie et al., 2008). A similar linear correlation between these two was also demonstrated by LES experiments in actual high-density urban areas and was further extended to the relationship between the velocity ratio and  $\lambda_f$  (Keck et al., 2014). These linear regressions are based on experimental measurements or simulations in actual urban areas, in which the effect from individual geometric parameters is difficult to identify due to irregular buildings and other obstacles and their complicated distributions in real cities. In this comprehensive parametric study, we demonstrate that a power regression in the form of Eq. (7) between the velocity ratio and aspect ratio may be more suitable. But to obtain a low aspect ratio for good ventilation, we need a relatively low building height ( $H$ ) and a wide parallel street width ( $W$ ). As  $\lambda_p$  has been concluded to be the most important factor, we herein focus on the other two targeted parameters,  $\lambda_f$  and  $P$ . After a few steps of derivation from Eqs. (1), (2), and (5), we can deduce that the aspect ratio is in inverse proportion to  $\lambda_f$ , but its relation with  $P$  is uncertain (it may be either positive or negative). A similar power law equation between  $\lambda_f$  and pedestrian wind speed was derived in a previous

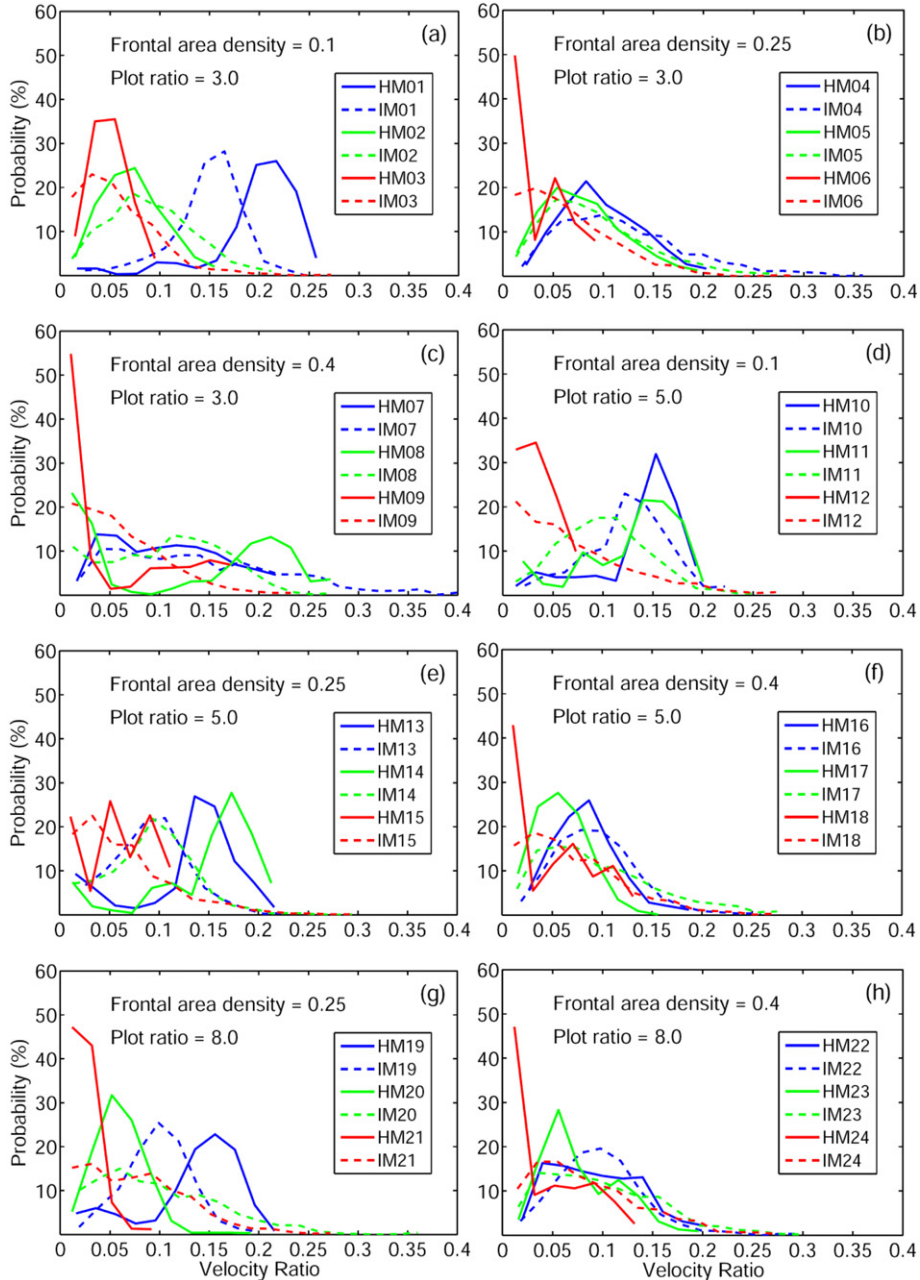


**Fig. 10.** Distributions of velocity ratios (referenced at 2 m above the ground) taken from random test points. Blue, green, and red lines denote a ground cover ratio of 25%, 50%, and 75%, respectively. Solid lines indicate homogeneous models, while dashed lines indicate inhomogeneous models.

parametric study (Razak et al., 2013), which suggested that  $\lambda_f$  is the product of  $\lambda_p$  and the building aspect ratio. Consequently, a good understanding of local microclimate, specifically prevailing wind direction in summer, is very important in urban planning and design in tropical and subtropical regions.

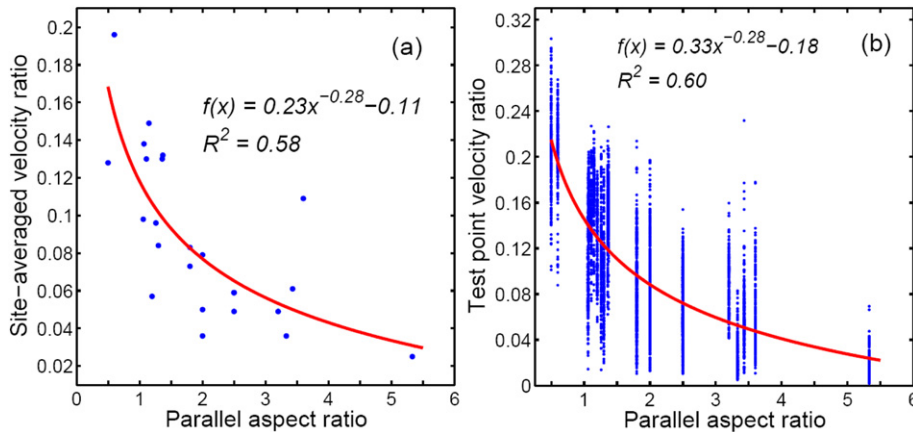


**Fig. 11.** Power regressions for aspect ratios of the parallel street canyons and velocity ratios in homogeneous scenarios. Velocity ratios in (a) are site-averaged and in (b) are randomly chosen (200 test points in each scenario) in the parallel streets with crossings excluded.

#### 4.3. Height differential and turbulent momentum

The power regression between velocity ratios and parallel aspect ratios is valid only for homogeneous scenarios. As can be seen when comparing Fig. 8 with Fig. 7, inhomogeneous building heights present enhanced spatial differences in velocity ratio. Relative high-rise buildings are generated from the normally distributed random series generator in inhomogeneous parametric scenarios, and it is obvious that on the windward side of high-rise buildings, pedestrian-level wind velocities are enhanced significantly (Fig. 8). Overall ventilation performance is thereby affected by building differentials. We compare the site-averaged velocity ratio in each pair of scenarios (the last two columns of Table 3) and summarize the results opposite the planning parameters in Table 4, which provides a cross-comparison of the influences of urban density and building height differentials on air ventilation.

One point that can be identified from Table 4 is that in most cases of either  $\lambda_p = 75\%$  or  $\lambda_f = 0.4$ , inhomogeneous building heights have better ventilation performance than homogeneous building heights. One exception is model number 08. But for this model, though the site-averaged velocity ratio is higher in HM08 than in IM08, their distributions in Fig. 10c (green lines) suggest that HM08 (solid green line) is not convincing, as it gives two extreme situations of ventilation: very good in the parallel streets and very bad in the perpendicular streets, with the highest probability of very low velocity ratios (below 0.03); hence IM08 (dashed green line) should be considered better. In cases of “HM is better,” both low  $\lambda_p$  (25%) and low  $\lambda_f$  (0.1) may be necessary. With medium values of  $\lambda_p$  (50%) or  $\lambda_f$  (0.25) in combination, the influence of building height differentials is case-dependent.

Fig. 12 further demonstrates the phenomenon deduced from Table 4. Site-averaged velocity ratios are averaged opposite various  $\lambda_p$  and  $\lambda_f$  conditions in Fig. 12. Figs. 12a and b show that in cases of low  $\lambda_f$  (0.1 or 0.25), homogeneous building height is better (provides larger mean site-averaged velocity ratio) when  $\lambda_p = 25\%$ , inhomogeneous building height is better when  $\lambda_p = 75\%$ , and the mean site-averaged velocity ratios are close when  $\lambda_p = 50\%$ . Fig. 12c demonstrates that in cases of  $\lambda_f = 0.4$ , inhomogeneous building height is always better than homogeneous. The averages of all  $\lambda_f$  values in Fig. 12d are consistent with the situations in Figs. 12a and b.

Dynamical potentials for these impacts of building height differentials on ventilation performance are of scientific merit. From the viewpoint of velocity level and vertical momentum flux in the urban canopy, horizontally averaged profiles of horizontal velocity components (Fig. 13) and the U-component of the total vertical momentum flux (Fig. 14) of all scenarios are herein investigated. The horizontal velocity components in Fig. 13 are normalized over the corresponding values at the free top ( $UV_{Top}$ ), and the vertical axes (Z) are normalized over the mean building height of all scenarios ( $H_{Mean}$ , approximately 36 m). They are shown only below  $3H_{Mean}$  (about 120 m), so that the differences among various scenarios at low levels of the urban canopy can be easily identified. Furthermore,  $\lambda_p$  values can be identified by colour in both Figs. 13 and 14: blue

profiles are scenarios of  $\lambda_p = 25\%$ , green profiles are scenarios of  $\lambda_p = 50\%$ , and red profiles are scenarios of  $\lambda_p = 75\%$ .

Roughly speaking, higher-density (larger  $\lambda_p$ ) scenarios have relatively stronger wind speeds in the upper levels. A possible explanation is that more momentum is conveyed to the lower levels in lower-density scenarios than in higher-density scenarios, which can be demonstrated by the domain-averaged total turbulent momentum profiles in Fig. 10. Negative values of these momentum fluxes indicate downward propagation of kinetic energy. Maximum momentum fluxes occur at around the heights of the building top in each scenario. Transitions of flow regimes with changes in urban density may occur, e.g., a transition from a “skimming” flow in higher-density scenarios to a “wake interference” flow in lower-density scenarios (Jiang et al., 2008; Kanda et al., 2004).

Downward-propagated momentum fluxes are generally stronger in IM scenarios than in HM scenarios when profiles in Fig. 14 c–d are compared with profiles in Fig. 14a–b. However, stronger vertical momentum flux in street canyons does not always mean more wind loads at the pedestrian level. Stronger vertical momentum flux means higher ventilation, which is the case for high-density scenarios. This can be recognized when comparing high-density parametric models (e.g.,  $\lambda_p = 75\%$ ) in HM scenarios in Fig. 7 with IM scenarios in Fig. 8. But stronger vertical momentum may cause lower ventilation in low-density parametric scenarios. An evident example is Figs. 7a and 8a, which demonstrate that height differential and stronger vertical momentum flux reduce pedestrian-level ventilation. An interesting finding for pedestrian-level ventilation from our simulations in and over generic urban configurations is that inhomogeneous building heights generate more vertical momentum in street canyons by capturing more downward-propagated momentum fluxes, and they have a negative (positive) effect on the pedestrian-level velocity of low-density (high-density) idealized urban fabrics. A similar phenomenon has been found in previous urban wind studies but with a focus on other parameters. For example, in a wind tunnel study of scalar (e.g., air mass) transfer efficiency, Ikegaya et al. (2012) pointed out that the transfer coefficients for arrays with blocks of inhomogeneous heights were smaller than for arrays with blocks of homogeneous heights under low  $\lambda_p$  conditions, but the opposite tendency was observed as  $\lambda_p$  increased. Dynamically, the decrease in the transfer coefficient in low  $\lambda_p$  conditions is due to the decrease in advection effects, which can be estimated from the larger values of drag coefficients for inhomogeneous arrays when compared with those of homogeneous arrays (Hagishima et al., 2009). In contrast, high-rise blocks in inhomogeneous arrays introduce more flow momentum into the canopy under high  $\lambda_p$  conditions (Ikegaya et al., 2012).

To further corroborate the above finding, we show the scatter plots between the site-averaged velocity ratios and vertical velocity averaged in the street canyons in Fig. 15. Fig. 15a shows scenarios of homogeneous building height (HM) with a higher site-averaged velocity ratio, while Fig. 15b shows scenarios of inhomogeneous building height (IM) with a higher site-averaged velocity ratio. The vertical velocity is averaged below 120 m to represent the vertical momentum in the street canyons. It is found that site-averaged velocity ratios present a negative relationship with the vertical velocity averaged in the street canyons in Fig. 15a, while the two show a positive relationship in Fig. 15b. Though the points are scattered, the negative and positive relations are obvious. The linear regressions (red lines) further demonstrate this opposite relation, from which we can deduce that inhomogeneous building heights generate more vertical momentum flux in the street canyons, resulting in deficits in horizontal advection effects and decreases in pedestrian-level ventilation in low-density scenarios, but more flow momentum into the street canyons with increases in pedestrian-level ventilation in high-density scenarios. Finally, the application of this point is that homogeneous building

**Table 4**

Influence of building height differential on ventilation performance. The first row is frontal area density, the last row is plot ratio, and the last column is ground coverage ratio. See text for detailed interpretations.

$\lambda_f$	0.1	0.25	0.4	0.1	0.25	0.4	0.25	0.4	$\lambda_p$
HM is better	01		08	10	13		19		25%
				11	14				50%
									75%
IM is better		04	07			16		22	25%
	02	05				17	20	23	50%
	03	06	09	12	15	18	21	24	75%
P	3			5			8		

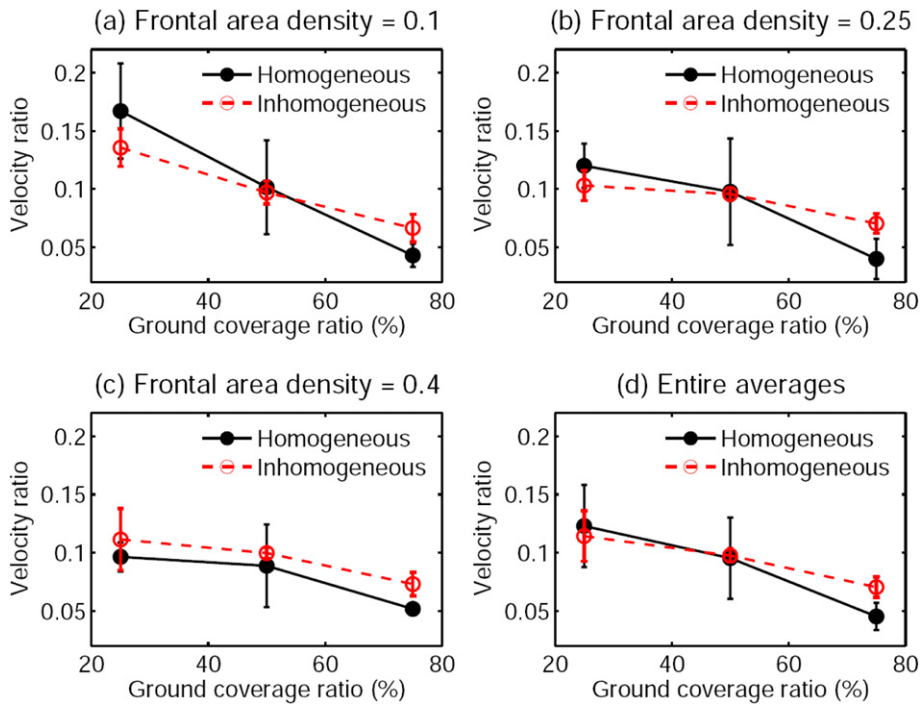


**Fig. 12.** Site-averaged velocity ratios under various ground coverage ratio ( $\lambda_p$ ) conditions and various frontal area density ( $\lambda_f$ ) conditions: (a)  $\lambda_f = 0.1$ , (b)  $\lambda_f = 0.25$ , (c)  $\lambda_f = 0.4$ , and (d) averages of all  $\lambda_f$  values. Homogeneous (black symbols) and inhomogeneous (red symbols) scenarios are averaged separately. The error bars represent one standard deviation.

heights are recommended when low density is present, and inhomogeneous building heights may be better in cases of high density.

## 5. Conclusions

This study investigates ventilation performance in parametric urban scenarios using an LES model—PALM. The PALM codes used in this study are first validated using the AIJ guidelines for CFD building simulations before being utilized in simulations of parametric scenarios. Four morphological parameters in urban design and planning, including ground coverage ratio ( $\lambda_p$ ), frontal area density ( $\lambda_f$ ), plot ratio ( $P$ ), and building height differential, are used to construct the parametric scenarios. Three values are set for each of these parameters except building height differential: 25%, 50%, and 75% for  $\lambda_p$ ; 0.1, 0.25, and 0.4 for  $\lambda_f$ ; and 3.0, 5.0, and 8.0 for  $P$ . For building height differential, we propose two situations: homogeneous and inhomogeneous. Homogeneous means all buildings are of the same height, while for inhomogeneous, building heights are generated by a normally distributed random series. With fixed site area, floor height, and floor area, a total of 54 scenarios can be obtained. Excluding 6 unrealistic cases, a total of 48 scenarios are investigated.

PALM-computed velocity ratios at 2 m above the ground, horizontally averaged velocity, and vertical momentum flux profiles in all scenarios are analyzed. The key findings and recommendations for urban planning deduced from this study are: First, among all four investigated parameters,  $\lambda_p$  is found to be the most important for good pedestrian-level ventilation. This conclusion we derived from Figs. 9 and 10 is somehow contributed by the prescribed values in Table 2. The significance of  $\lambda_p$  and  $\lambda_f$  for urban ventilation were widely examined, but the fact is that a real city or urban area is complex, and a single idealized parameter will probably fail to capture the complex impacts of building geometries on air flows. The potential combined effects of different parameters led to the follow-up analysis and conclusions. Second, in the case of homogeneous

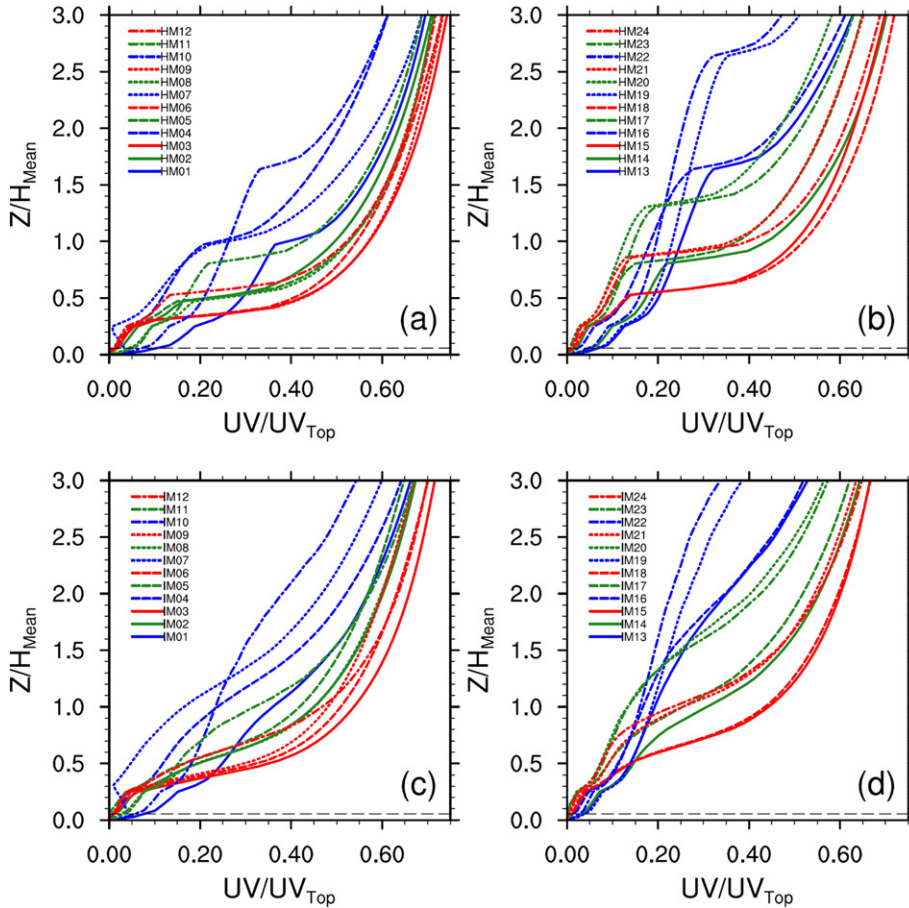


**Fig. 13.** Horizontally averaged profiles of horizontal velocity components ( $(U^2 + V^2)^{1/2}$ , abbreviated as UV here) of all 48 scenarios. The velocity values are normalized over the corresponding values at the free top ( $UV_{Top}$ ), and the vertical axes ( $Z$ ) are normalized over the mean building height of all scenarios ( $H_{Mean}$ , approximately 36 m). Blue lines denote scenarios with a  $\lambda_p$  value of 25%, green lines denote scenarios with a  $\lambda_p$  value of 50%, and red lines denote scenarios with a  $\lambda_p$  value of 75%.

building heights, a power regression between velocity ratios and aspect ratios of street canyons that are parallel to the inflow direction can be derived. The samples (scatter points) for the regressions in Fig. 11 are rather scattered, which may be due to the limitation of such a parametric study. That is, we can simulate only a few values for each parameter, as adding one value to every single parameter would require substantial additional LES experiments and computational capacity. But this power regression is at least more representative than a linear relation, and agreement can be found with previous studies, e.g., Razak et al. (2013). This concluding remark suggests that good understanding of local microclimate, in particular prevailing wind directions in summer, is very important in urban planning. Third, the effects of building height differential on urban ventilation are connected with urban density: In relatively low-density scenarios, inhomogeneous building heights give worse ventilation performance compared to homogeneous cases; in a few medium- to high-density scenarios, ventilation performances of homogeneous and inhomogeneous building heights are close and complex; and in high-density scenarios, inhomogeneous building heights result in better ventilation performance than homogeneous cases. An explanation of this phenomenon is that inhomogeneous building

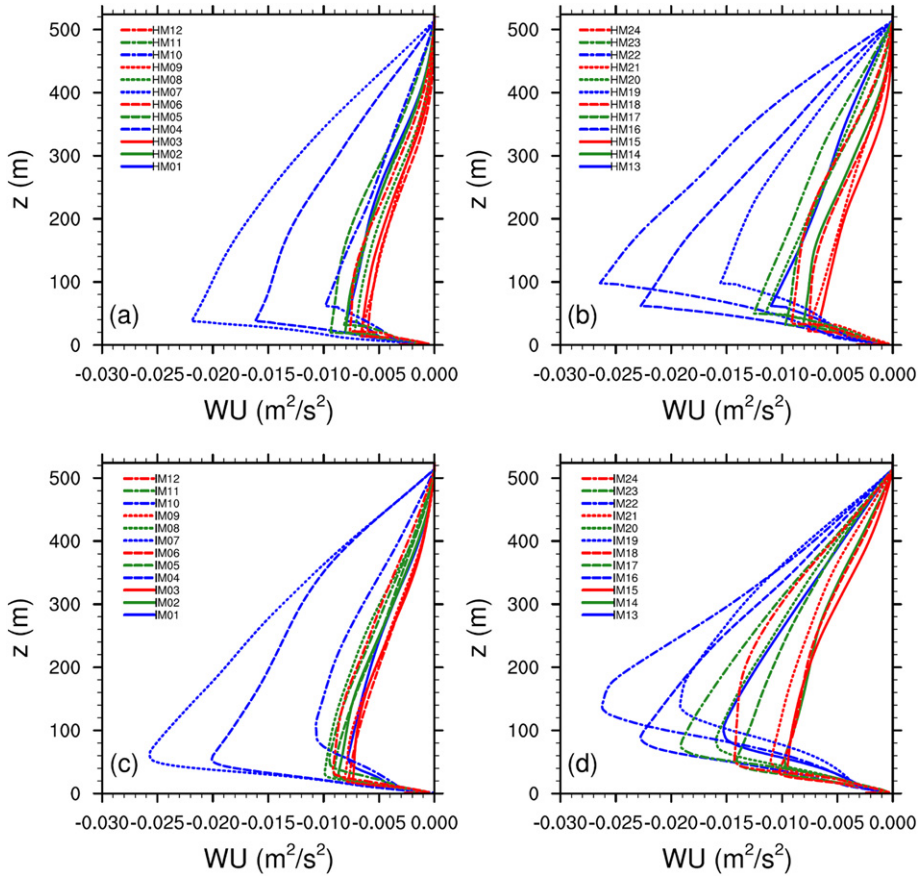


**Fig. 14.** Same as Fig. 13 but for the U-component of the total vertical momentum flux (WU) profiles up to the top level without normalization.

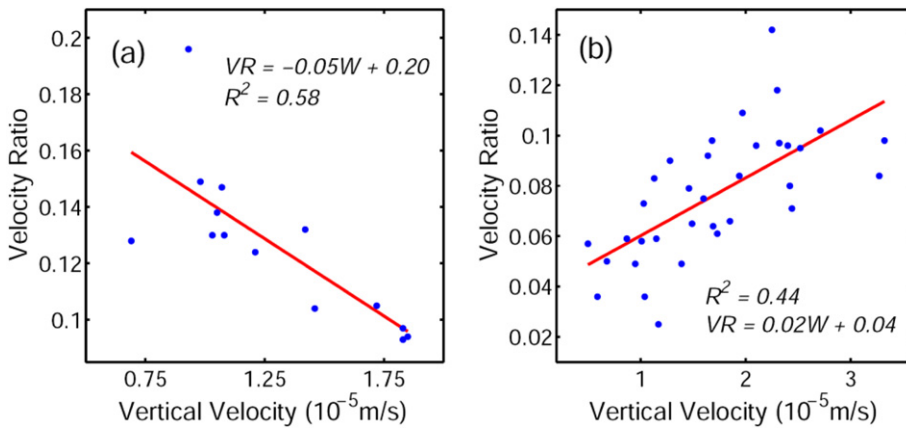


**Fig. 15.** Scatter plot of site-averaged velocity ratios (VR) against vertical velocity ( $W$ ) averaged in the street canyons below 120 m in scenarios of (a) homogeneous building height (HM) with higher site-averaged velocity ratio, and (b) inhomogeneous building height (IM) with higher site-averaged velocity ratio. The red lines represent linear regressions.

heights generate more vertical momentum flux in the street canyons, resulting in deficits in horizontal advection effects and decreases in pedestrian-level ventilation in low-density scenarios, but more flow momentum into the street canyons and increases in pedestrian-level ventilation in high-density scenarios. The application of this point is that homogeneous building heights are recommended when low density ( $\lambda_p$  and  $\lambda_f$ ) is present, and inhomogeneous building heights may be better in cases of high density.

## Acknowledgments

This study was supported by the Research Grants Council of the Hong Kong Special Administrative Region (Project No. 14408214), and Institute of Environment, Energy and Sustainability, The Chinese University of Hong Kong (Project ID: 1907002).

## References

- Arakawa, A., Lamb, V.R., 1977. Computational design of the basic dynamical processes of the UCLA general circulation model. In: Chang, J. (Ed.), *General Circulation Models of the Atmosphere, Methods in Computational Physics*, pp. 173–263 Berlin.
- Britter, R.E., Hanna, S.R., 2003. Flow and dispersion in urban areas. *Annu. Rev. Fluid Mech.* 35 (1), 469–496.
- Buccolieri, R., Salizzoni, P., Soulhac, L., Garbero, V., Di Sabatino, S., 2015. The breathability of compact cities. *Urban Climate* 13, 73–93.
- Castillo, M.C., Inagaki, A., Kanda, M., 2011. The effects of inner- and outer-layer turbulence in a convective boundary layer on the near-neutral inertial sublayer over an urban-like surface. *Bound.-Lay. Meteorol.* 140 (3), 453–469.
- Chen, Q., 2009. Ventilation performance prediction for buildings: a method overview and recent applications. *Build. Environ.* 44 (4), 848–858.
- Deardorff, J.W., 1980. Stratocumulus-capped mixed layers derived from a three-dimensional model. *Bound.-Lay. Meteorol.* 18, 495–527.
- Hagishima, A., Tanimoto, J., Nagayama, K., Meno, S., 2009. Aerodynamic parameters of regular arrays of rectangular blocks with various geometries. *Bound.-Lay. Meteorol.* 132 (2), 315–337.
- Hang, J., Luo, Z., Sandberg, M., Gong, J., 2013. Natural ventilation assessment in typical open and semi-open urban environments under various wind directions. *Build. Environ.* 70, 318–333.
- Harlow, F.H., Welch, J.E., 1965. Numerical calculation of time-dependent viscous incompressible flow of fluid with free surface. *Phys. Fluids* 8, 2182–2189.
- Ho, Y.-K., Liu, C.-H., Wong, M.S., 2015. Preliminary study of the parameterisation of street-level ventilation in idealised two-dimensional simulations. *Build. Environ.* 89, 345–355.
- Hunter, L.J., Johnson, G.T., Watson, I.D., 1992. An investigation of three-dimensional characteristics of flow regimes within the urban canyon. *Atmos. Environ.* 20, 425–432.
- Ikegaya, N., Hagishima, A., Tanimoto, J., Tanaka, Y., Narita, K.-i., Zaki, S. A., 2012. Geometric dependence of the scalar transfer efficiency over rough surfaces. *Bound.-Lay. Meteorol.* 143 (2), 357–377.
- Inagaki, A., Castillo, M.C.L., Yamashita, Y., Kanda, M., Takimoto, H., 2011. Large-eddy simulation of coherent flow structures within a cubical canopy. *Bound.-Lay. Meteorol.* 142 (2), 207–222.
- IPCC, 2013. Summary for policymakers. In: Stocker, T.F., Qin, D., Plattner, G.-K., Tignor, M., Allen, S.K., Boschung, J., Nauels, A., Xia, Y., Bex, V., Midgley, P.M. (Eds.), *Climate Change 2013: The Physical Science Basis. Contribution of Working Group I to the Fifth Assessment Report of the Intergovernmental Panel on Climate Change*. Cambridge University Press, Cambridge, United Kingdom and New York, NY, USA.
- Jiang, D., Jiang, W., Liu, H., Sun, J., 2008. Systematic influence of different building spacing, height and layout on mean wind and turbulent characteristics within and over urban building arrays. *Wind Struct.* 11 (4), 275–289.
- Kanda, M., Moriawaki, R., Kasamatsu, F., 2004. Large-eddy simulation of turbulent organized structures within and above explicitly resolved arrays. *Bound.-Lay. Meteorol.* 112, 343–368.
- Kanda, M., Inagaki, A., Miyamoto, T., Gryschka, M., Raasch, S., 2013. A new aerodynamic parameterization for real urban surfaces. *Bound.-Lay. Meteorol.* 148 (2), 357–377.
- Keck, M., Raasch, S., Letzel, M.O., Ng, E., 2014. First results of high resolution large-eddy simulations of the atmospheric boundary layer. *Journal of Heat Island Institute International* 9 (2), 39–43.
- Lam, C.Y., 2006. On climate changes brought about by urban living. *Hong Kong Meteorological Society Bulletin* 16 (1/2), 55–61.
- Letzel, M.O., Krane, M., Raasch, S., 2008. High resolution urban large-eddy simulation studies from street canyon to neighbourhood scale. *Atmos. Environ.* 42 (38), 8770–8784.
- Letzel, M.O., Helmke, C., Ng, E., An, X., Lai, A., Raasch, S., 2012. LES case study on pedestrian level ventilation in two neighbourhoods in Hong Kong. *Meteorol. Z.* 21 (6), 575–589.
- Leung, Y.K., Wu, M.C., Yeung, K.K., Leung, W.M., 2007. Temperature projections in Hong Kong based on IPCC fourth assessment report. *Hong Kong Meteorological Society Bulletin* 17, 1–23.
- Leung, Y.K., Yip, K.M., Yeung, K.H., 2008. Relationship between thermal index and mortality in Hong Kong. *Meteorol. Appl.* 15 (3), 399–409.
- Lin, M., Hang, J., Li, Y., Luo, Z., Sandberg, M., 2014. Quantitative ventilation assessments of idealized urban canopy layers with various urban layouts and the same building packing density. *Build. Environ.* 79, 152–167.
- Lo, K.W., Ngan, K., 2015. Characterising the pollutant ventilation characteristics of street canyons using the tracer age and age spectrum. *Atmos. Environ.* 122, 611–621.
- Maronga, B., Gryschka, M., Heinze, R., Hoffmann, F., Kanani-Sühring, F., Keck, M., Ketelsen, K., Letzel, M.O., Sühring, M., Raasch, S., 2015. The Parallelized Large-Eddy Simulation Model (PALM) version 4.0 for atmospheric and oceanic flows: model formulation, recent developments, and future perspectives. *Geosci. Model Dev. Discuss.* 8 (2), 1539–1637.

- Mirzaei, P.A., Haghighat, F., 2010. A novel approach to enhance outdoor air quality: pedestrian ventilation system. *Build. Environ.* 45 (7), 1582–1593.
- Mochida, A., Tominaga, Y., Murakami, S., Yoshie, R., Ishihara, T., Ooka, R., 2002. Comparison of various  $k-\epsilon$  models and DSM applied to flow around a high-rise building – report on AIJ cooperative project for CFD prediction of wind environment. *Wind Struct.* 5, 227–244.
- Moeng, C.H., Wyngaard, J.C., 1988. Spectral analysis of large-eddy simulations of the convective boundary layer. *J. Atmos. Sci.* 45 (23), 3573–3587.
- Nazarian, N., Kleissl, J., 2016. Realistic solar heating in urban areas: air exchange and street-canyon ventilation. *Build. Environ.* 95, 75–93.
- Ng, E., 2009. Policies and technical guidelines for urban planning of high-density cities – air ventilation assessment (AVA) of Hong Kong. *Build. Environ.* 44 (7), 1478–1488.
- Ng, E., Cheng, V., 2012. Urban human thermal comfort in hot and humid Hong Kong. *Energ. Buildings* 55, 51–65.
- Ng, E., Yuan, C., Chen, L., Ren, C., Fung, J.C.H., 2011. Improving the wind environment in high-density cities by understanding urban morphology and surface roughness: a study in Hong Kong. *Landsc. Urban Plan.* 101 (1), 59–74.
- Oke, T.R., 1988. Street design and urban canopy layer climate. *Energ. Buildings* 11, 103–113.
- Park, S.-B., Baik, J.-J., 2014. Large-eddy simulations of convective boundary layers over flat and urbanlike surfaces. *J. Atmos. Sci.* 71 (5), 1880–1892.
- Park, S.-B., Baik, J.-J., Raasch, S., Letzel, M.O., 2012. A large-eddy simulation study of thermal effects on turbulent flow and dispersion in and above a street canyon. *J. Appl. Meteorol. Climatol.* 51 (5), 829–841.
- Piacsek, S.A., Williams, G.P., 1970. Conservation properties of convection difference schemes. *J. Comput. Phys.* 198, 580–616.
- Raasch, S., Schröder, M., 2001. PALM - a large-eddy simulation model performing on massively parallel computers. *Meteorol. Z.* 10, 363–372.
- Ramponi, R., Blocken, B., de Co, L.B., Janssen, W.D., 2015. CFD simulation of outdoor ventilation of generic urban configurations with different urban densities and equal and unequal street widths. *Build. Environ.* 92, 152–166.
- Razak, A.A., Hagishima, A., Ikegaya, N., Tanimoto, J., 2013. Analysis of airflow over building arrays for assessment of urban wind environment. *Build. Environ.* 59, 56–65.
- Rodi, W., Ferziger, J.H., Breuer, M., Pourquié, M., 1997. Status of large eddy simulation: results of a workshop. *J. Fluids Eng.* 119 (2), 248–262.
- Saiki, E.M., Moeng, C.H., Sullivan, P.P., 2000. Large-eddy simulation of the stably stratified planetary boundary layer. *Bound.-Lay. Meteorol.* 95, 1–30.
- Schumann, U., 1975. Subgrid scale model for finite difference simulations of turbulent flows in plane channels and annuli. *J. Comput. Phys.* 18, 376–404.
- Skote, M., Sandberg, M., Westerberg, U., Claesson, L., Johansson, A., 2005. Numerical and experimental studies of wind environment in an urban morphology. *Atmos. Environ.* 39 (33), 6147–6158.
- Tamura, T., 2008. Towards practical use of LES in wind engineering. *J. Wind Eng. Ind. Aerodyn.* 96 (10–11), 1451–1471.
- Temperton, C., 1992. A generalized prime factor FFT algorithm for any  $N = 2^3 \cdot 5^t$ . *SIAM J. Sci. Stat. Comput.* 13, 676–686.
- Tominaga, Y., Mochida, A., Yoshie, R., Kataoka, H., Nozu, T., Yoshikawa, M., Shirasawa, T., 2008. AIJ guidelines for practical applications of CFD to pedestrian wind environment around buildings. *J. Wind Eng. Ind. Aerodyn.* 96, 1749–1761.
- Wang, W., Zhou, W., Ng, E.Y.Y., Xu, Y., 2016. Urban heat islands in Hong Kong: statistical modeling and trend detection. *Nat. Hazards* 83 (2), 885–907.
- Wicker, L.J., Skamarock, W.C., 2002. Time-splitting methods for elastic models using forward time schemes. *Mon. Weather Rev.* 130, 2088–2097.
- Williamson, J.H., 1980. Low-storage Runge-Kutta schemes. *J. Comput. Phys.* 35, 48–56.
- Yang, L., Li, Y., 2011. Thermal conditions and ventilation in an ideal city model of Hong Kong. *Energ. Buildings* 43 (5), 1139–1148.
- Yang, F., Qian, F., Lau, S.S.Y., 2013. Urban form and density as indicators for summertime outdoor ventilation potential: a case study on high-rise housing in Shanghai. *Build. Environ.* 70, 122–137.
- Yoshie, R., Tanaka, H., Shirasawa, T., Kobayashi, T., 2008. Experimental study on air ventilation in a built-up area with closely-packed high-rise buildings. *Journal of Environmental Engineering (Transactions of AIJ)* 73, 661–667.
- Yuan, C., Ng, E., 2012. Building porosity for better urban ventilation in high-density cities – a computational parametric study. *Build. Environ.* 50, 176–189.
- Yuan, C., Ng, E., 2014. Practical application of CFD on environmentally sensitive architectural design at high density cities: a case study in Hong Kong. *Urban Climate* 8, 57–77.
- Yuan, C., Ng, E., Norford, L.K., 2014. Improving air quality in high-density cities by understanding the relationship between air pollutant dispersion and urban morphologies. *Build. Environ.* 71, 245–258.